

How curvature flows: scaling laws and global geometry of impact induced attrition processes

Gergő Pál,^{1,2} Gábor Domokos,^{3,4} and Ferenc Kun^{1,*}

¹*Department of Theoretical Physics, Doctoral School of Physics, Faculty of Science and Technology, University of Debrecen, P.O. Box 400, H-4002 Debrecen, Hungary*

²*Institute of Nuclear Research (Atomki), P.O. Box 51, H-4001 Debrecen, Hungary*

³*Department of Mechanics, Materials and Structures, Budapest University of Technology and Economics, Műegyetem rkp. 3., K261, 1111 Budapest, Hungary*

⁴*MTA-BME Morphodynamics Research Group, Műegyetem rkp. 3., K261, 1111 Budapest, Hungary*

(Dated: October 6, 2021)

Impact induced attrition processes are, beyond being essential models of industrial ore processing, broadly regarded as the key to decipher the provenance of sedimentary particles. A detailed understanding of single impact phenomena of solid bodies has been obtained in physics and engineering, however, the description of gradual mass reduction and shape evolution in impact sequences relies on approximate mathematical models of mean field type, formulated as curvature-driven partial differential equations. Here we establish the first link between microscopic, particle-based material models and the mean field theory for these processes. Based on realistic computer simulations of particle-wall collision sequences, we first identify the well-known damage and fragmentation energy phases, then we show that the former is split into the *abrasion phase* with infinite sample lifetime, analogous to Sternberg's Law, at finite asymptotic mass and the *cleavage phase* with finite sample lifetime, decreasing as a power law of the impact velocity, analogous to Basquin's Law. We demonstrate that only in the abrasion phase does shape evolution emerging in microscopic material models reproduce with startling accuracy the spatio-temporal patterns predicted by macroscopic mean field approaches. Our results substantially extend the phase diagram of impact phenomena and set the boundaries of the applicability of geometric mean field theories for geological shape evolution. Additionally, the scaling laws obtained can be exploited for quantitative predictions of evolution histories.

I. INTRODUCTION

Impact induced damage and fragmentation of solids is ubiquitous in nature and plays a crucial role in the evolution of our geological environment: repeated impacts shape particles (sand grains, pebbles, and volcanic rocks) in sediment transport [1–9], affect the production of ash and pyroclast particles in volcanic eruptions [10, 11], and contribute to the generation of atmospheric aerosols with consequences on air pollution and on the global climate [12]. In the Solar system, the size and shape of asteroids and of the particles of planetary rings observed today are the results of a long lasting collisional evolution [13–17]. On planet Mars traces of fluvial evolution of landforms such as pebbles have been discovered [5, 18] similar to river beds on Earth. Particle breakage is widely used by the industry in comminution processes of ores and minerals [19–23], however, it can also be undesired in process and handling engineering due to the resulting degradation of product quality. In these natural processes and industrial applications particles collide both with each other and with hard walls presented by Earth surface (river beds, beaches, and rock walls) or by the components of the process equipment (conveyors, transporta-

tion tubes, and containers).

Over the past decades, detailed knowledge has been accumulated in geology [1, 2, 18, 24], physics [25–28, 28, 29, 29–32], and engineering [19, 23, 33–35] on single impact breakage phenomena, however, a comprehensive understanding of low velocity impact sequences responsible for the gradual mass reduction and global rounding of solid particles is still lacking. In the physics literature the existence of two distinct *energy phases* (the *damage phase* and the *fragmentation phase*) has been established not only for brittle materials [29, 31, 33, 36], and plastics spheres [37], but also for liquid droplets [38]. Moreover, the same two energy phases have also been reported in the geophysics literature [8] for the collisional attrition of sedimentary particles. In the latter context, global mechanical and geometric understanding of impact induced breakage would be essential to decipher the information hidden in the size and shape of grains and pebbles [1–4, 18]. While research in geology and physics concentrated on single impact phenomena, mathematical research related to the proof of the Poincaré conjecture [39–41] led to the study of a class of nonlinear geometric partial differential equations (PDEs) called *curvature-driven flows* which appear to be the adequate mean-field theory models for the global evolution of pebbles and other particles under a large number of low energy impacts [42, 43]. One may target global shape evolution of particles either by extending the physics literature about single breakage to multiple breakage processes or by re-

*Electronic address: Corresponding author: ferenc.kun@science.unideb.hu

lying on mean field PDE models. Although the latter are invaluable tools to obtain qualitative insight, nevertheless, their application has not yet been rigorously justified: until now there existed no theory linking microscopic and macroscopic approaches, in particular, there were no clear physical criteria established for the breakage process which would admit mean field PDEs as valid global approximations.

The latter, on the other hand, appear to be very useful as they make specific geometric predictions: global evolution starting from cuboid polyhedra (serving as averaged models of natural fragments [24, 44]) occurs in two *geometric phases*: in the first (local rounding) phase vertices and edges become rounded but axis ratios hardly change while in the second (global rounding) phase roundness remains almost constant while axis ratios increase [9, 45]. These geometric phases have been identified both in laboratory experiments and in numerical simulations of the PDEs [9, 46] and this naturally led to the hypothesis that the geometric phases may also exist in a mechanical abrasion model. In stark contrast to geometric shape evolution of pebbles, *no phases* can be distinguished in the evolution of mass [9] which appears to obey Sternberg's empirical law of exponential decay, approaching zero at infinite time [47].

Here we present a thorough theoretical study of the phase structure of impact induced attrition processes with the primary aim to establish a firm link between microscopic physical breakage models and macroscopic (mean field) geometric PDE models. Based on realistic discrete element simulations of sequences of particle-wall collisions, we show that, depending on the impact velocity, the first (damage) energy phase may be clearly separated *into two further energy phases*, so there exist three distinct energy phases: at sufficiently low velocities repeated impacts result in abrasion of the body and lead to a finite asymptotic residual mass (*abrasion phase*), however, above a threshold velocity a complete destruction is achieved within a finite number of repetitions (*cleavage phase*). Instantaneous fragmentation occurs above a second critical velocity where cracks span the entire body and the sample rapidly falls apart into a large number of small pieces (*fragmentation phase*). The transitions between the abrasion, cleavage, and fragmentation phases occur at well-defined critical velocities analogous to continuous phase transitions.

We establish the link between microscopic physical breakage models and mean-field PDEs in two steps. First, the splitting of the earlier identified damage phase into the abrasion and cleavage phases delineates the range of validity for the latter: the main feature of the now identified abrasion phase is that each impact removes only a small amount of (relative) mass. As PDE models are based on the limit where the removed relative mass in each collision approaches zero, our study shows that PDEs can be regarded as a mean field approximation of collision-induced attrition in the abrasion energy phase. Second, we identify one key feature of the PDE model

in the microscopic simulation: we show that two *geometric phases* earlier identified in the context of the PDE model clearly emerge inside the abrasion phase in the microscopic breakage model.

Our finding is based on large scale computer simulations which revealed that the evolution of the mass and shape of the solid is governed by scaling laws in terms of the impact velocity. Most notably, in the abrasion phase the shape evolution of the sample is described by a universal scaling form with a power law dependence on the impact velocity predicting infinite sample lifetime at some finite, asymptotic mass, the latter being determined by the energy threshold for the creation of cracks. In the special limit when this threshold approaches zero, our findings reproduce Sternberg's Law [47], predicting exponential decay (and infinite lifetime) for sedimentary particles undergoing collisional abrasion in fluvial environments. In addition to verify Sternberg's Law for mass evolution, in the energetic abrasion phase we also confirmed the existence of the two earlier observed *geometric phases* [9, 45], thus our simulations serve as the first direct mechanical confirmation of curvature-driven PDEs as models of impact-driven abrasion processes. In the cleavage phase we find that the sample lifetime decreases as a power law of the impact velocity analogous to the Basquin law [48, 49] of sub-critical fracture.

II. SINGLE IMPACTS: TRANSITION FROM DAMAGE TO FRAGMENTATION

To understand the evolution of solid bodies under repeated collisions with a hard wall, first we focus on single impact events and quantify the resulting mass reduction. We performed numerical measurements by means of computer simulations of a realistic discrete element model (DEM) of body-wall collisions in three dimensions (3D) [50–54] varying the impact velocity v_0 in a broad range. To represent freshly fractured rocks with sharp corners and edges in the initial state of shape evolution, rectangular samples of mildly elongated cubic shape were created with the aspect ratio 1 : 1.2 : 1.4 of their shortest c_0 , intermediate b_0 , and longest a_0 sides. This choice is justified by our recent finding that the average shape of fragments is well approximated by a cube for a large diversity of fragmentation processes [44].

In the model the sample is represented as a random packing, consisting, on the average, of 12.000 spherical particles with a uniformly distributed diameter d in a narrow interval Δd around the average $\langle d \rangle$ with $\Delta d / \langle d \rangle = 0.05$ [52]. Cohesive interaction is realized by beam elements which connect the particles along the edges of Delaunay triangles constructed from the initial particle positions [50, 51, 55]. During the impact process in three dimensions (3D), the total deformation of a beam is calculated as the superposition of elongation, torsion, as well as, bending and shearing [29, 56]. Cracks are formed when overstressed beams break according to a

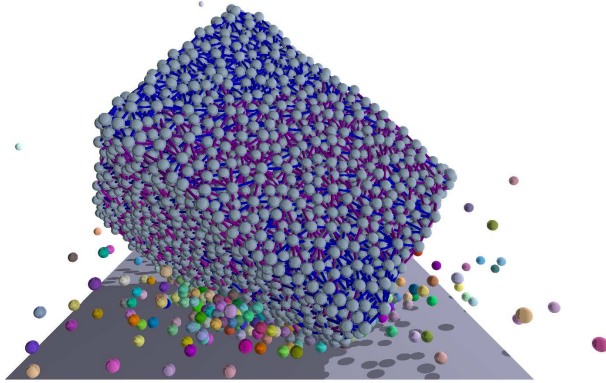


Figure 1: A snapshot of the time evolution of the first impact of a sample with a hard wall. The initially angular body hits the wall close to one of its corners. Most of the fragments are single particles flying at a high speed. Colors are randomly assigned to the fragments. The intact cohesive contacts are represented by lines connecting the spherical particles.

physical breaking rule. The breaking condition takes into account the stretching and shearing of particles contacts

$$\left(\frac{\varepsilon_{ij}}{\varepsilon_{th}}\right)^2 + \frac{\max(\Theta_i, \Theta_j)}{\Theta_{th}} \geq 1, \quad (1)$$

where ε_{ij} denotes the axial strain of the beam between particles i and j , while Θ_i , and Θ_j are the bending angles of the beam ends. The parameters ε_{th} and Θ_{th} control the relative importance of the two breaking modes [29, 31, 50, 51, 57]. The breaking criterion is evaluated after each iteration step and those beams which fulfill the condition are removed from the system. In the model there is only structural disorder present, i.e. the breaking thresholds are constant $\varepsilon_{th} = 0.02$ and $\Theta_{th} = 3^\circ$, however, the physical properties of beams such as length, cross section, and elastic moduli, are determined by the random particle packing. At the broken beams along the surface of the spheres cracks are generated inside the solid and as a result of the successive beam breaking the solid falls apart. The interaction of those particles which are not connected by beams, e.g. because the beam has been broken, is described by the Hertz contact law [58]. The time evolution of the impacting body is generated by solving the equation of motion of all the particles. Parameters of the model were set in such a way that our DEM provides a consistent qualitative and in certain cases quantitative description of the mechanical and fracture properties of the broad class of heterogeneous brittle materials which are abundant in our geological environment (see Table I). The model has been successfully applied before to investigate fracture and fragmentation under various types of loading conditions [50–53].

Initially, the discretized sample was placed close to a planar wall with a random orientation chosen uniformly

Table I: Parameters of the discrete element model.

Beams:				
longitudinal stiffness	E^b	6	GPa	
strain threshold	ε_{th}	0.02	-	
bending threshold	θ_{th}	3	degree	
Particles:				
stiffness	E^p	3	GPa	
Average diameter	$\langle d \rangle$	0.5	mm	
density	ρ	3000	kg/m ³	
Hard wall:				
stiffness	E^w	70	GPa	
Interaction:				
friction coefficient	μ	1	-	
damping coefficient (normal)	γ_n	0.25	s ⁻¹	
friction coefficient (tangential)	γ_t	0.05	s ⁻¹	
System:				
time increment	Δt	1e-7	s	
average number of particles	N^p	12000	-	
average number of beams	N^b	105000	-	
solid fraction		0.65	-	
Macroscopic properties (DEM):				
system stiffness	E	7.4 ± 0.5	GPa	
Poisson's ratio	ν	0.2	-	
system strength	σ_c	110	MPa	

on the sphere and the impact was initiated by assigning identical velocity v_0 perpendicular to the wall to all particles of the solid. As the body moved, it got into contact with the wall and deformed which could result in cracking and fragment formation. The impact lasted until complete rebound was achieved where all particles separated from the wall. In the final state of the process, particles connected by the surviving cohesive elements were identified as fragments. A snapshot of the impact process is presented in Fig. 1.

Simulations revealed that for sufficiently low impact velocities $v_0 < v_a$ the sample solely underwent deformation around the impact site and rebounded elastically without suffering any damage. Cracks first occurred when v_0 surpassed a threshold velocity v_a determined by the strength of the internal cohesive elements of the material. In this low velocity range, deformation and crack formation is restricted to the vicinity of the contact zone, while for high impact velocities cracks can span the entire sample giving rise to rapid breakup. To give a quantitative characterization of the final outcome and the degree of destruction caused by impacts, we determined the average masses M_{1st} and M_{2nd} of the largest and second largest fragments, respectively. After normalizing these values by the total mass M_0 we plotted $m_{1st} = \langle M_{1st}/M_0 \rangle$, $m_{2nd} = \langle M_{2nd}/M_0 \rangle$ as function of the impact velocity v_0 . It can be observed in Fig. 2 that at low impact velocities we have $m_{2nd} \ll m_{1st}$, i.e. the second largest fragment is orders of magnitude smaller than the largest one, showing that only small pieces are removed from the body around the impact site. This is characteristic for the *damage energy phase*. Fragmenta-

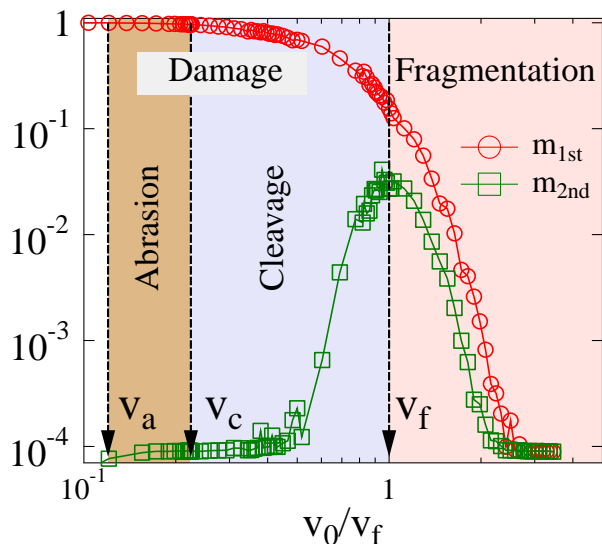


Figure 2: The three energy phases. Mass of the largest m_{1st} and second largest m_{2nd} fragments obtained after a single impact as function of the impact velocity v_0 . In the regime $v_0 < v_a$ of low velocities no cracking occurs and the impactor elastically rebounds from the wall. In the abrasion phase $v_a < v_0 < v_c$ small fragments are removed from the body by chipping. To achieve complete breakup in a single impact, v_0 has to exceed the critical fragmentation velocity v_f . In the intermediate velocity range $v_c < v_0 < v_f$ of cleavage, cracks penetrate deeper inside splitting larger pieces from the body. The critical velocity v_c of cleavage is the threshold velocity above which the asymptotic remaining mass tends to zero in repeated collisions. Horizontal axis shows on logarithmic scale the impact velocity v_0 normalized by critical fragmentation velocity v_f . For the model solid we found the (non-dimensional) ratio of threshold velocities to be $v_a/v_f = 0.124$. and $v_c/v_f = 0.224$.

tion is achieved when the second largest piece becomes comparable to the largest one, which first occurs at the maximum of m_{2nd} defining the critical velocity v_f of fragmentation. Beyond the *critical fragmentation velocity* v_f both m_{1st} and m_{2nd} decrease monotonically. Figure 2, illustrating the phase diagram of impact induced attrition processes, shows that, depending on the velocity, single impacts give rise either to damage or fragmentation of the sample with a sharp transition at the critical velocity v_f . The damage - fragmentation transition has already been studied in experiments and computer simulations of impacting spherical samples against a hard wall, using heterogeneous brittle materials [29, 31, 33, 36], plastics spheres [37], and liquid droplets [38]. In these studies, the same qualitative behavior was obtained for the largest fragment masses m_{1st} , m_{2nd} as in Fig. 2, which implies that the overall outcome of the process in the high velocity range is entirely controlled by the impact velocity and its critical value v_f , whereas neither the sample's shape nor materials' features have any relevant effect. The detailed analysis of the mass distribution of fragments re-

vealed that the observed universality is caused by the underlying continuous phase transition from damage to fragmentation as the impact velocity is varied [25, 38, 59]. The identification of the known damage and fragmentation phases also serves as a verification of our model.

III. REPEATED IMPACTS AND THE TWO SUB-PHASES OF DAMAGE: ABRASION AND CLEAVAGE

In the previous subsection, confirming earlier results, we established for single impact phenomena the existence of the two main energy phases. Now we will show that, if we consider not just a single impact but impact *sequences*, the damage phase can be subdivided into two narrower energy phases: abrasion and cleavage. The damage phase, characterized by $v_0 \ll v_f$ is often observed in natural and industrial processes at lower energy levels. Under such conditions, the large residue of the sample typically undergoes repeated collisions which give rise to a complex evolution of its size and shape. In the following we extend the global phase diagram of Fig. 2 refining the structure of the damage phase by characterizing qualitatively different evolution histories of residues under *repeated* sub-critical impacts.

To simulate sequences of particle-wall collisions, in the final state of an impact event we identified the largest fragment as the residue of the body. It was then replaced by its counterpart cut out of the initial sample, to ensure an undeformed, relaxed initial state for the subsequent collision. The residue was randomly rotated in three dimensions and was impacted against the wall with the same impact velocity $v_0 < v_f$ as before. The above procedure was repeated up to $N_{max} = 400$ times, or until complete destruction of the body, at ≈ 60 different impact velocities, respectively. For each sequence, 120 different initial samples were used, while in subsequent impacts the residues were randomly rotated by uniformly choosing a direction on the sphere. These calculations revealed an astonishingly rich phase structure of the sub-critical $v_0 < v_f$ regime.

To quantify the gradual mass reduction during the collision sequence, Figure 3(a) presents the average $m_r = \langle M_r/M_0 \rangle$ of the residual mass M_r normalized by the initial mass of the sample M_0 , as a function of the impact number N for several values of v_0 . (We remark that for a single impact event we have $m_r \equiv m_{1st}$.) At very low velocities $v_0 \ll v_f$, a single impact always gives rise only to a few fragments which are typically single spheres, i.e. powder in the model. As a consequence, in Fig. 3(a) the residual mass m_r gradually decreases with increasing impact number N , however, mass reduction gets limited for high N values and a finite asymptotic residual mass emerges $m_r \rightarrow m_r^a$ as $N \rightarrow \infty$. The reason is that due to the decreasing mass M_r , the kinetic energy $E_0 = \frac{1}{2}M_r v_0^2$, imparted to the sample decreases, since the impact velocity v_0 is fixed. Consequently, beyond a certain impact

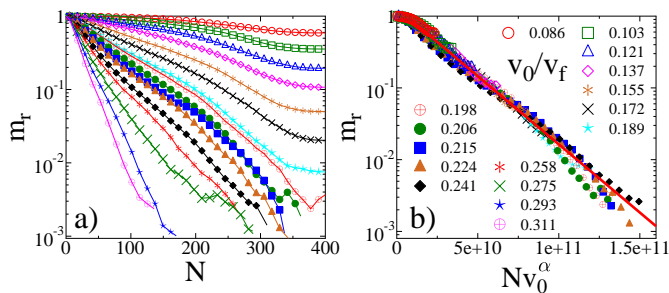


Figure 3: (a) Average mass of the residue m_r as a function of the impact number N for several impact velocities v_0 below the fragmentation critical point v_f . Panel (b) shows that by rescaling the horizontal axis, curves of different v_0 values can be collapsed onto one single master curve. Note that data of the lowest impact velocities (highest remaining mass) are in the upper left corner at the start of the master curve. Straight line represents the exponential form of the scaling function $\tilde{m}_r(x)$ of Eq. (2). The legend for (a) and (b) is given in (b).

number (i.e. below a certain value of M_r), the emerging deformation is not sufficient to induce further cracking.

Since only small pieces are removed in single impacts, we term this velocity regime as the *abrasion phase* of the system characterized by the existence of a finite asymptotic residual mass $m_r^a > 0$. It can be observed in Fig. 3(a) that the value of m_r^a decreases with increasing impact velocity v_0 . The value of m_r^a depends also on the energy threshold for the creation of cracks, i.e. on the strength of cohesive contacts. In the limit when this threshold approaches zero, our findings reproduce Sternberg's Law [47], predicting exponential decay to zero mass and infinite lifetime for sedimentary particles undergoing collisional abrasion in fluvial environments.

When v_0 gets sufficiently high, the functional form of $m_r(N)$ qualitatively changes: the mass of the residue sets to a rapid decrease with N , and repeated impacts give rise to a complete destruction of the sample within a finite number of repetitions. This behavior is characterized by impact velocities in the range $v_c < v_0 < v_f$ and we call this interval the *cleavage phase* of the impact sequence. The critical velocity v_c of cleavage is defined as the threshold velocity above which the asymptotic residual mass is zero even at finite energy threshold for the creation of cracks. In our discrete element model, a complete destruction of the sample is reached when the largest fragment comprises solely a single particle of the discretization. For real materials this state is realized when the residual size approaches a characteristic length scale of the meso-structure, e.g. grain size of materials.

The transition from abrasion to cleavage at the critical velocity v_c is driven by the changing mechanism of cracking. In the abrasion phase the dominating mechanism of mass removal is chipping, i.e. crack formation parallel to the contact surface with the wall, which leads to the formation of tiny fragments [60, 61]. However, in the case of cleavage, cracks penetrate the solid to signif-

icantly deeper regions so that a combination of contact damage and fracture occurs, giving rise to coarser products as well. Additionally, the elastic waves generated by the collision give rise to the gradual accumulation of damage inside the residue which, in turn, can result in fatigue crack growth as the impact sequence proceeds [62].

Our results demonstrate that above the threshold velocity of micro-cracking v_a , impact attrition phenomena have additionally two well-defined critical impact velocities v_c and v_f , which separate the three phases of abrasion, cleavage, and fragmentation with distinct qualitative behaviors (see the phase diagram of Fig. 2). For our model solid, the threshold velocities of abrasion and cleavage are $v_a/v_f = 0.124 \pm 0.004$ and $v_c/v_f = 0.224 \pm 0.005$, with respect to the fragmentation critical velocity v_f .

A. Sternberg's law and Basquin's law

Figure 3(b) demonstrates that rescaling the impact number N with a proper power α of v_0 , curves belonging to different impact velocities v_0 can be collapsed on the top of each other, yielding the scaling form

$$m_r(N, v_0) = \tilde{m}_r(Nv_0^\alpha), \quad (2)$$

where the scaling function $\tilde{m}_r(x)$ can be approximated by an exponential $\tilde{m}_r(x) \sim \exp(-x)$ (see Fig. 3(b)), reproducing the time evolution predicted by Sternberg's law [47]. Best collapse is achieved in Fig. 3(b) with the exponent $\alpha = 2.1 \pm 0.15$.

It follows from the scaling analysis that increasing the impact velocity v_0 the characteristic impact number N_c of the time evolution decreases as a power law

$$N_c \sim v_0^{-\alpha}. \quad (3)$$

The scaling law Eq. (3) holds in both the abrasion and cleavage phases $v_a < v_0 < v_f$ of impact attrition. For cleavage, the characteristic impact number N_c can be interpreted as the lifetime of the sample. Since the peak stress, emerging at the contact zone during impact, increases as a power of the impact velocity v_0 [63], it follows that the expression (3) of residual lifetime is analogous to the Basquin law of sub-critical fracture phenomena [48, 49, 64–66]. The Basquin law of fatigue life is a fundamental law of sub-critical fracture. It expresses that under a constant or varying sub-critical load, where the stress amplitude falls below the fracture strength of materials, failure occurs in a finite time which decreases as a power law of the externally applied stress amplitude [48]. Our results demonstrate that the Basquin law holds also for sub-critical impact phenomena.

In the abrasion phase N_c characterizes the rate of convergence to the asymptotic residual mass m_r^a . Additionally, the impact velocity also determines the value of m_r^a , which tends to zero when approaching the critical point v_c from below, see Fig. 4 which also shows (inset) that

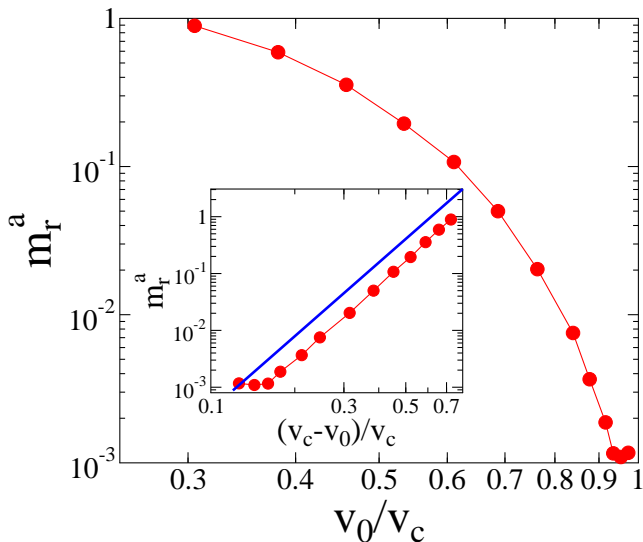


Figure 4: Asymptotic mass m_r^a of the residue as a function of the impact velocity in the abrasion phase $v_0 < v_c$. Inset: the mass values of the main panel are re-plotted as a function of the relative distance from the critical point v_c . The straight line represents a power law of exponent $\beta = 4.2$.

the convergence to zero is well described by a power law as a function of the distance from the critical point

$$m_r^a \sim (v_c - v_0)^\beta, \quad \text{for } v_0 \leq v_c. \quad (4)$$

For the exponent we obtained $\beta = 4.2 \pm 0.2$ by fitting of data. Since in the cleavage phase we have $m_r^a = 0$, whereas in the abrasion phase we have $m_r^a > 0$, m_r^a can be considered as the order parameter of the abrasion-cleavage phase transition, and β is the order parameter exponent of the transition.

IV. SHAPE EVOLUTION: GEOMETRIC PHASES INSIDE THE ABRASION ENERGY PHASE

A. Mean field models

In case of polyhedral initial samples, in the abrasion phase we expect that at the beginning of the impact sequence sharp corners and edges are gradually removed, giving rise to an evolution towards an asymptotic rounded shape. In the cleavage phase, due to the breaking of coarser pieces, this evolution is more erratic and eventually results in an ultimate destruction. Due to the small size of fragments, we expect that geometric aspects of the abrasion phase may be well reflected in the solutions of averaged, mean field geometric PDE models of attrition [42, 43]. The simplest, two-dimensional version of these PDE models may be written as

$$V = c\kappa, \quad (5)$$

where V denotes the speed by which a surface points moves inward along the surface normal, κ is the scalar curvature and equation (5) is often referred to [39, 40] as the *curve shortening flow* or as the geometric heat equation. The constant c can be regarded as scaling of time and plays no role if evolution is plotted as a function of the normalized residual mass m_r . (We remark that equation (5) is written in a compact, invariant notation, details about this and other notations are given in Section 1 of the Supplemental Material [67].) Next we will show that these expectations are well founded and PDE models serve indeed as good approximations of impact-induced attrition processes, however, only in the abrasion phase.

B. Shape descriptors

To give a quantitative characterization of the rounding process, we picked three dimensionless descriptors of the overall shape of the residue (thus neglecting morphological details of its surface) which not only provide efficient monitoring of the geometric evolution but also admit meaningful comparison with earlier results: axis ratios, circularity (isoperimetric ratio) and intact surface ratio.

1. *Axis ratios* c/a and b/a are traditional geological descriptors [9] characterizing the shape of the residue [24, 68] where $a > b > c$ refer to the axes of the bounding box of the residue, aligned with the edges of the initial (cuboid) sample.
2. *Isoperimetric ratio* or circularity of a planar object is given as $R = 4\pi A/P^2$, where A, P refer to area and perimeter, respectively. It has been observed [8] that circularity of the largest projection of sedimentary particles shows universal features in fluvial abrasion and its evolution is entirely determined by the mass loss during impact induced attrition processes. In our DEM, A and P of the residue were obtained as the area and perimeter of the convex hull of the point cloud of the largest projection of the spherical particles of the relaxed body. For more details on shape descriptors see Section 3 of the Supplemental Material [67].
3. *Intact surface ratio* S/S_0 , expressing the intact fraction of the initial surface, was selected following an idea of Richard Hamilton [45] who, in one of the papers dedicated to the study of curvature-driven flows (leading ultimately towards to his seminal contribution to the proof of the Poincaré - conjecture) describes a curious nonlinear phenomenon about intact surface ratio in the Gauss curvature flow which is the 3D version of (5): he predicted that S/S_0 will drop to zero after a finite time, marking the end of the first geometric phase for cuboids. (For more details see Section 4 of the Supplemental Material [67].) In the initial state of DEM samples

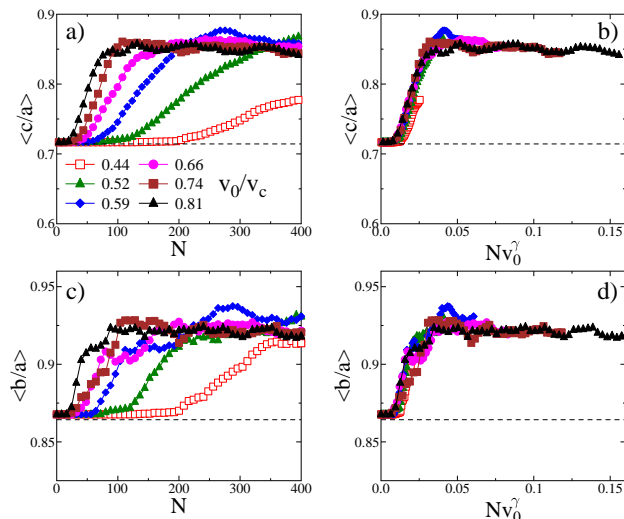


Figure 5: Average side length ratios $\langle c/a \rangle$ (a) and $\langle b/a \rangle$ (c) of the bounding box of the residues as function of the impact number N for different impact velocities inside the abrasion energy phase $v_0 < v_c$. The horizontal dashed lines represent the initial values $\langle c_0/a_0 \rangle = 1/1.4$ and $\langle b_0/a_0 \rangle = 1.2/1.4$. By rescaling the impact number N in (b) and (d) by an appropriate power γ of the impact velocity v_0 , the curves of different v_0 of (a) and (c) can be collapsed on master curves. Best collapse is achieved using the same exponent $\gamma = 3$ in (b) and (d).

S_0 is determined as the number of particles covering the external body surface, then the surviving intact surface S is obtained by tracing the particles removed from the initial surface S_0 in subsequent impacts.

The evolution of axis ratios c/a and b/a and the evolution of the isoperimetric ratio R has been computed in the PDE model [9] for the very same cuboid initial conditions as in our DEM study. For the evolution of intact surface ratio S/S_0 in the PDE model we have an analytical result [45]. We will now establish the link between PDE models and microscopic computations by comparing these evolutions. The most striking qualitative feature of the PDE model is the spontaneous emergence of two *geometric phases* and our computations reveal that these phases are perfectly captured in the microscopic DEM approach. To make the comparison between plots for shape descriptors meaningful, next we seek the corresponding scaling laws.

C. Scaling laws

Increasing v_0 accelerates mass removal and thus shape evolution. Figures 5(a, c) demonstrate that both axis ratios $\langle c/a \rangle(N, v_0)$, $\langle b/a \rangle(N, v_0)$ remain initially constant, display sudden growth between the characteristic impact

numbers N_r and N_s and subsequently saturate. Both the overall shape of these functions and their saturation values remain the same in the entire abrasion phase, however both N_r and N_s decrease with increasing v_0 . We found that rescaling these curves with v_0^γ , they collapse onto master curves (see Fig. 5(b, d)) implying the scaling structure

$$\langle c/a \rangle(N, v_0) = \Phi(Nv_0^\gamma), \quad (6)$$

$$\langle b/a \rangle(N, v_0) = \Psi(Nv_0^\gamma), \quad (7)$$

where $\Phi(x)$ and $\Psi(x)$ denote the scaling functions. This also implies that N_r and N_s both have the same power law dependence

$$N_r \approx Av_0^{-\gamma}, \quad N_s \approx Bv_0^{-\gamma}, \quad (8)$$

where the exponent γ was obtained numerically $\gamma = 3.0 \pm 0.07$. The saturation values $\langle c/a \rangle \approx 0.865$ and $\langle b/a \rangle \approx 0.925$ show that the asymptotic stable shape of the object is slightly anisotropic which may be a consequence of the finite number of the non-breakable discrete elements in the simulation. Our simulations revealed that under the condition of isotropic impacts, the origin of the universal scaling forms is that the shape of the evolving object is controlled by the total relative mass $\mu(N) = 1 - m_r$ lost in N repeated collisions. Recently, it has been suggested [8] that $\mu(N)$ is also controlling the evolution of the circularity R , so henceforth we use this representation for all shape descriptors.

D. Geometric phases

The PDE model (5) predicts for the evolution of cuboid blocs with moderate initial axis ratios the emergence of two geometric phases: in phase 1 axis ratios $c/a, b/a$ remain approximately constant while roundness increases steeply and saturates close to 1. In phase 2 the opposite happens: axis ratios increase steeply and saturate close to 1 while roundness remains constant. The conceptual plot of this evolution (as a function of the relative abraded mass $\mu = 1 - m_r$) is shown in Figure 6(b1), accompanied by conceptual contours of the specimen, projected along the shortest (c) axis (b2) and representative snapshots of DEM simulations (b3). Figure 6(c1) shows the same plot for b/a and R , obtained from the numerical computation [9] of the PDE (5). Figure 6(c2) presents the hand-drawn sketch of Hamilton [45] of his analytical result on the same PDE: intact surface area S/S_0 survives for a finite time and this marks geometric phase 1.

In Figure 6(a) we compare the DEM computations to the aforementioned analytical predictions. In Figure 6(a1) we show evolutions of the average axis ratio $\langle b/a \rangle$ and roundness $\langle R \rangle$ in the abrasion energy phase $v_a < v_0 < v_c$. Note that curves of different impact velocities all fall on the top of each other in agreement with the scaling collapse predicted in the previous section. It is apparent that we have good qualitative agreement with Figure 6(c1): $\langle b/a \rangle$ remains constant at the

initial value $\langle b/a \rangle = 1.2/1.4$ until $\mu^* \approx 0.34$ while $\langle R \rangle$ increases sharply and the opposite can be observed for $\mu > 0.34$. Based on this observations we can clearly

record the presence of the two geometric phases in the abrasion energy phase for the evolutions of the axis ratios and the roundness.

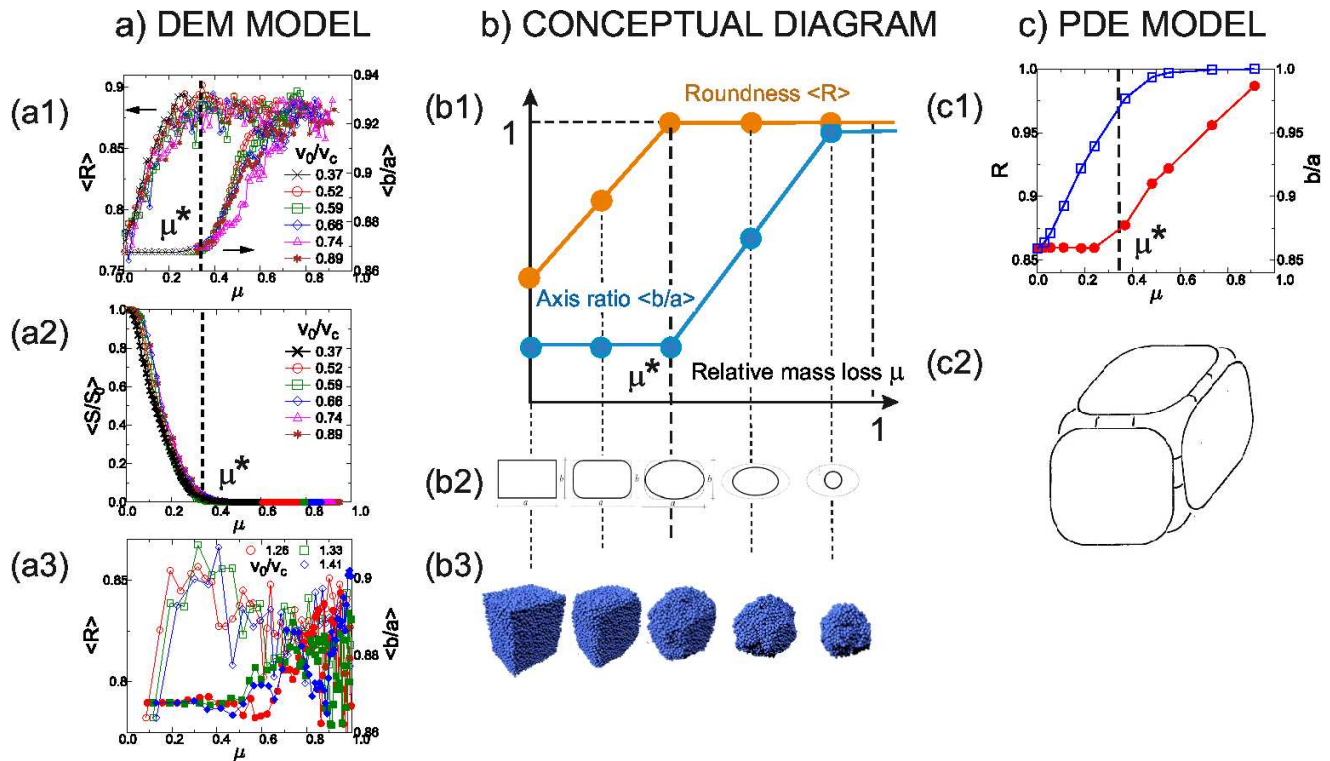


Figure 6: Geometric shape evolution as a function of the relative abraded mass μ . (a) DEM simulations: (a1) Abrasion energy phase: evolution of the average circularity $\langle R \rangle$ and axis ratio $\langle b/a \rangle$. Observe two geometric phases: phase 1 with approximately constant $\langle b/a \rangle$ followed by phase 2 with approximately constant $\langle R \rangle$. Transition at $\mu^* \approx 0.34$. (a2) Abrasion energy phase: evolution of intact surface ratio S/S_0 . Transition between phases at $\mu^* \approx 0.34$. (a3) Cleavage phase: evolution of the average circularity $\langle R \rangle$ (open symbols) and axis ratio $\langle b/a \rangle$ (filled symbols). Observe absence of smooth evolution. (b1) Schematic, bilinear approximation of two-phase geometric evolution of axis ratios and roundness. (b2) Schematic side view of abrading cuboids, projected along the shortest (c) axis. (b3) Snapshots of DEM simulations. (c) PDE model results: (c1) Evolution of circularity R and axis ratio b/a [9]. Observe two geometric phases: phase 1 with approximately constant b/a followed by phase 2 with approximately constant R . (c2) Hand-drawn sketch by R. Hamilton [45] predicting phase 1 characterized by nonzero intact surface ratio.

In Figure 6(a2) we show the evolution of the intact surface ratio S/S_0 , also in the abrasion energy phase $v_a < v_0 < v_c$. We can observe that this shape descriptor drops to zero at the same relative abraded mass value ($\mu^* \approx 0.34$) which separates the two phases for the evolution of axis ratios and roundness. This is in agreement with the prediction of Hamilton [45] who claimed that intact surface area will survive for a finite time. It is easy to see that as long as intact surface area exists, the corresponding axis ratio of the cuboid (computed from the bounding box) will remain constant so here again we see a perfect match between the DEM computations and the prediction based on the PDE. The transition point μ^* between the two geometric phases in the microscopic DEM and macroscopic mean field PDE descriptions of shape evolution have a very good agreement.

This confirms our claim that in the abrasion energy

phase $v_a < v_0 < v_c$ the PDE model offers adequate description of the shape evolution. In sharp contrast, Figure 6(a3) illustrates the evolution of the axis ratio b/a and roundness R in the cleavage energy phase $v_c < v_0 < v_f$, both displaying a non-smooth behavior: here we do not expect any mean-field PDE model to provide an adequate description.

V. DISCUSSION

Impact induced attrition processes cover a broad variety of phenomena ranging from the gentle removal of fine powder from the surface of rock pieces by low velocity impacts to the immediate disruption of objects in energetic collisions. Understanding gradual mass removal due to a sequence of impact events is crucial in sedimentol-

ogy since pebbles can be considered as witnesses of the geological conditions of their creation. Universal scaling laws of lifetime, size, and shape of evolving particles are indispensable to decode the information imprinted in pebbles [1–4, 18]. In the initial state of this evolution process freshly fragmented rocks are generated [24] by dynamic breakup of rock masses due to high velocity impacts. While the theory of single impact of solid particles with a hard wall is well understood at the level of particle-based models, impact sequences have been so far only modeled by mean field theory which necessarily included gross simplifications of the breaking process. Here we offered the first link between particle-based models and mean field theory for collision sequences.

The main methodological novelty of our study is that we use the discrete element method to realistically simulate the entire physical process of all the individual impacts of long sequences without any additional assumption. Although at high computational costs (by simulating $\approx 5 \times 10^5$ collisions with samples consisting of $\approx 12,000$ discrete elements), this approach enabled us to unveil the rich phase structure of impact induced attrition processes. Based on experimental observations, a descriptive classification of single impact breakage has been proposed in [19], where low, intermediate, and high velocity ranges were distinguished according to the amount and structure of the resulting damage of the body. Here we demonstrated that in multiple impact processes these regimes are separated by universal phase transitions. In addition to the already known damage and fragmentation phases (separated by the critical impact velocity v_f) we identified the abrasion and cleavage phases *inside* the damage phase (separated by the critical velocity v_c). Abrasion results in finite asymptotic mass (analogous to Sternberg’s Law [47]) while cleavage results in a complete destruction after a finite number of impacts, with sample lifetime decreasing as a power law of the impact velocity (analogously to Basquin’s law).

By identifying the abrasion energy phase we were able to provide the link between microscopic, particle-based models and mean-field curvature-driven equations. We showed that the latter can be regarded as adequate approximations of the former, however, only in the abrasion phase. Our simulations revealed an astonishing universality of the evolution of rounding of the residue. Both the axis ratios and the circularity of the largest projection proved to be entirely determined by the attrition mass: evolutions at different impact velocities v_0 can be collapsed onto a single curve by rescaling the number of impacts with a proper power α (also called the *lifetime exponent*) of v_0 . This universality confirmed earlier conjectures and observations [8, 9] on the existence of two geometric phases and also helped to identify a scaling law of the dynamics: the characteristic event number of the onset of shrinking of initially angular objects proved to decrease as a power law of the impact velocity. We were also able to verify a curious effect of geometric nonlinearity, first predicted by Hamilton [45]: in case of polyhedral

initial shapes, a finite amount of the initial surface area survived abrasion for a finite amount of time.

Our findings also fit into the broader picture of efforts to approximate PDE models by microscopic, particle-based simulations. In the context of curvature-driven surface evolution, closest to our current topic, Monte-Carlo simulations of the Kardar-Parisi-Zhang (KPZ) equation proved to be a powerful tool to understand the global dynamics [69, 70]. However, in contrast to our approach, discrete KPZ models do not use a mechanics-based DEM Kernel and most often they are aimed at surface growth in an orthogonal $[xyz]$ frame.

It is important to emphasize that the excellent qualitative and quantitative agreement (e.g. for the transition point between the two geometric phases) of the microscopic DEM and macroscopic PDE descriptions of shape evolution were obtained without any parameter tuning of DEM simulations. This confirms the high degree of robustness of the results for the broad class of heterogeneous brittle materials. For the initial state of shape evolution we considered mildly anisotropic cuboids, since it has proven to be the generic average shape of freshly fractured rocks [44]. Cuboids with other axis ratios would only change the time scale of shape evolution and shift the transition point μ^* between the geometric phases. Inside the energy phases of abrasion and cleavage, the temporal evolution of mass and shape is controlled by the impact velocity which we could cast into scaling laws. The value of the scaling exponent of lifetime (cleavage) α falls close to 2, while the exponent γ controlling the shape evolution (abrasion) has a higher value $\gamma \approx 3$. Based on fracture mechanics, approximate analytical expressions have been derived for the threshold velocities of the onset of abrasion v_a and fragmentation v_f [61]. These calculations showed that the critical velocities separating the energy phases of impact attrition phenomena depend on material properties as well as on the mass and linear extension of the sample [61]. Based on the analogy to continuous phase transitions, we conjecture that the critical exponents α , β , and γ are universal, they depend neither on mechanical, nor on geometrical features of the system.

Acknowledgments

The authors thank András Sipos for his invaluable help with computing Figure 6(c1). The work is supported by the EFOP-3.6.1-16-2016-00022 project. The project is co-financed by the European Union and the European Social Fund. This research was supported by the National Research, Development and Innovation Fund of Hungary, financed under the K-16 funding scheme Projects no. K 119967 and K 119245. The research reported in this paper at the Budapest University of Technology and Economics has been supported by the NRDI Fund, TKP2020 IES, Grant No. TKP2020 BME-IKA-VIZ. The research at the University of Debrecen was supported by the The-

-
- [1] Q. R. Wald, *Nature* **345**, 211 (1990).
- [2] M. S. Lorang and P. D. Komar, *Nature* **347**, 433 (1990).
- [3] D. L. Turcotte, *Fractals and chaos in geology and geophysics* (Cambridge University Press, 1997).
- [4] D. J. Durian, H. Bideaud, P. Düringer, A. Schröder, F. Thalmann, and C. M. Marques, *Phys. Rev. Lett.* **97**, 028001 (2006).
- [5] R. M. E. Williams, J. P. Grotzinger, W. E. Dietrich, S. Gupta, D. Y. Sumner, R. C. Wiens, N. Mangold, M. C. Malin, K. S. Edgett, S. Maurice, et al., *Science* **340**, 1068 (2013).
- [6] M.-L. Doan and G. Gary, *Nature Geoscience* **2**, 709 (2009), ISSN 1752-0908.
- [7] J. Dufek, M. Manga, and A. Patel, *Nature Geoscience* **5**, 561 (2012), ISSN 1752-0908.
- [8] T. Novák-Szabó, A. A. Sipos, S. Shaw, D. Bertoni, A. Pozzebon, E. Grottoli, G. Sarti, P. Ciavola, G. Domokos, and D. J. Jerolmack, *Science Advances* **4**, eaao4946 (2018).
- [9] G. Domokos, D. Jerolmack, A. Sipos, and A. Török, *PLoS ONE* **9**, e88657 (2014).
- [10] T. J. Jones and J. K. Russell, *Sci Rep* **7**, 1 (2017).
- [11] A. J. Hornby, Y. Lavallée, J. E. Kendrick, G. Rollinson, A. R. Butcher, S. Clesham, U. Kueppers, C. Cimarelli, and G. Chigna, *Sci Rep* **9**, 1 (2019).
- [12] J. F. Kok, *Proceedings of the National Academy of Sciences* **108**, 1016 (2011).
- [13] K. A. Dahmen, Y. Ben-Zion, and J. T. Uhl, *Nat. Phys.* **7**, 554 (2011).
- [14] P. Farinella and V. Zappalà, *Advances in Space Research* **19**, 181 (1997), proceedings of the E1.1, B1.5, and C2.4 Symposia of COSPAR Scientific Commissions E, B and C.
- [15] D. D. Durda, A. C. Bagatin, R. A. Aleman, G. J. Flynn, M. M. Strait, A. N. Clayton, and E. B. Patmore, *Planetary and Space Science* **107**, 77 (2015).
- [16] G. Domokos, A. Á. Sipos, G. M. Szabó, and P. L. Várkonyi, *The Astrophysical Journal* **699**, L13 (2009).
- [17] G. Domokos, A. Á. Sipos, G. M. Szabó, and P. L. Várkonyi, *Research Notes of the AAS* **1**, 50 (2017).
- [18] T. Szabó, G. Domokos, J. P. Grotzinger, and D. J. Jerolmack, *Nature Communications* **6**, 8366 (2015).
- [19] A. Salman, G. Reynolds, J. Fu, Y. Cheong, C. Biggs, M. Adams, D. Gorham, J. Lukenics, and M. Hounslow, *Powder Technology* **143-144**, 19 (2004), ISSN 0032-5910, particle Breakage.
- [20] B. A. Wills and J. A. Finch, in *Wills' Mineral Processing Technology (Eighth Edition)*, edited by B. A. Wills and J. A. Finch (Butterworth-Heinemann, Boston, 2016), pp. 109 – 122, eighth edition ed., ISBN 978-0-08-097053-0.
- [21] F. Spahn, E. V. Neto, A. H. F. Guimarães, A. N. Gorban, and N. V. Brilliantov, *New Journal of Physics* **16**, 013031 (2014).
- [22] N. Brilliantov, P. L. Krapivsky, A. Bodrova, F. Spahn, H. Hayakawa, V. Stadnichuk, and J. Schmidt, *Proceedings of the National Academy of Sciences* **112**, 9536 (2015).
- [23] E. Andrews and K.-S. Kim, *Mechanics of Materials* **31**, 689 (1999), ISSN 0167-6636.
- [24] G. Domokos, F. Kun, A. A. Sipos, and T. Szabó, *Scientific Reports* **5**, 9147 (2015).
- [25] F. Kun and H. J. Herrmann, *Phys. Rev. E* **59**, 2623 (1999).
- [26] H. Katsuragi, D. Sugino, and H. Honjo, *Phys. Rev. E* **68**, 046105 (2003).
- [27] T. Kadono, M. Arakawa, and N. Mitani, *Phys. Rev. E* **72**, 045106(R) (2005).
- [28] J. A. Aström, *Adv. Phys.* **55**, 247 (2006).
- [29] H. A. Carmona, F. K. Wittel, F. Kun, and H. J. Herrmann, *Phys. Rev. E* **77**, 051302 (2008).
- [30] Y. Wang and F. Tonon, *International Journal of Rock Mechanics and Mining Sciences* **48**, 535 (2011), ISSN 1365-1609.
- [31] G. Timár, F. Kun, H. A. Carmona, and H. J. Herrmann, *Phys. Rev. E* **86**, 016113 (2012).
- [32] Y. Ye, K. Thoeni, Y. Zeng, O. Buzzi, and A. Giacomini, *Rock Mechanics and Rock Engineering* (2019).
- [33] G. Ma, W. Zhou, Y. Zhang, Q. Wang, and X. Chang, *Powder Technology* **325**, 498 (2018).
- [34] N. Arbiter, C. Harris, and G. A. Stamboltzis, *Transactions of the Society of Mining Engineers, AIME* **244**, 118 (1969).
- [35] K. T. Chau, X. X. Wei, R. H. C. Wong, and T. X. Yu, *Mechanics of Materials* **32**, 543 (2000).
- [36] N. Myagkov, *Physica A: Statistical Mechanics and its Applications* **534**, 122117 (2019).
- [37] G. Timár, J. Blömer, F. Kun, and H. J. Herrmann, *Phys. Rev. Lett.* **104**, 095502 (2010).
- [38] C. F. Moukarzel, S. F. Fernandez-Sabido, and J. C. Ruiz-Suarez, *Phys. Rev. E* **75**, 061127 (2007).
- [39] M. Gage and R. Hamilton, *J. Differ. Geom.* **23**, 69 (1986).
- [40] M. Grayson, *J. Differ. Geom.* **26**, 285 (1987).
- [41] G. Perelman, ArXiv preprint <https://arxiv.org/abs/math/0303109> (2003).
- [42] W. Firey, *Mathematika* **21**, 1 (1974).
- [43] F. J. Bloore, *Math. Geol.* **9**, 113 (1977).
- [44] G. Domokos, D. J. Jerolmack, F. Kun, and J. Török, *Proceedings of the National Academy of Sciences* **117**, 18178 (2020).
- [45] R. Hamilton, *Discourses Math. Appl.* **3**, 69 (1994).
- [46] D. Priour Jr., ArXiv preprint <https://arxiv.org/abs/2003.03476> (2020).
- [47] H. Sternberg, *Zeitschrift für Bauwesen* **25**, 483 (1875).
- [48] O. H. Basquin, *Proceedings of American Society of Testing Materials ASTEA* **10**, 625 (1910).
- [49] F. Kun, H. A. Carmona, J. S. Andrade Jr., and H. J. Herrmann, *Phys. Rev. Lett.* **100**, 094301 (2008).
- [50] F. Kun, I. Varga, S. Lennartz-Sassinek, and I. G. Main, *Phys. Rev. E* **88**, 062207 (2013).
- [51] F. Kun, I. Varga, S. Lennartz-Sassinek, and I. G. Main, *Phys. Rev. Lett.* **112**, 065501 (2014).
- [52] G. Pál, I. Varga, and F. Kun, *Phys. Rev. E* **90**, 062811 (2014).
- [53] G. Pál, Z. Jánosi, F. Kun, and I. G. Main, *Phys. Rev. E* **94**, 053003 (2016).
- [54] G. Pál and F. Kun, *Granular Matter* **18**, 74 (2016).

- [55] F. Kun, G. Pál, I. Varga, and I. G. Main, Philosophical Transactions of the Royal Society A: Mathematical, Physical and Engineering Sciences **377**, 20170393 (2019).
- [56] F. Wittel, H. Carmona, F. Kun, and H. Herrmann, Int J Fract **154**, 105 (2008).
- [57] F. Kun and H. J. Herrmann, Comp. Meth. Appl. Mech. Eng. **138**, 3 (1996).
- [58] F. Radjai and F. Dubois, *Discrete-element modeling of granular materials* (Wiley-Iste, 2011), ISBN 1848212607.
- [59] T. Kadono, Phys. Rev. Lett. **78**, 1444 (1997).
- [60] J. Subero and M. Ghadiri, Powder Technology **120**, 232 (2001).
- [61] M. Ghadiri and Z. Zhang, Chemical Engineering Science **57**, 3659 (2002), ISSN 0009-2509.
- [62] H. J. Herrmann and S. Roux, eds., *Statistical models for the fracture of disordered media*, Random materials and processes (Elsevier, Amsterdam, 1990).
- [63] K. L. Johnson, *Contact Mechanics* (Cambridge University Press, New York, 1985).
- [64] S. Suresh, *Fatigue of Materials* (Cambridge University Press, 1998).
- [65] D. Sornette, T. Magnin, and Y. Brechet, Europhys. Lett. **20**, 433 (1992).
- [66] A. P. Vieira, J. S. Andrade, and H. J. Herrmann, Phys. Rev. Lett. **100**, 195503 (2008).
- [67] *Supplemental material*.
- [68] L. M. L. Pen, W. Powrie, A. Zervos, S. Ahmed, and S. Aingaran, Granular Matter **15**, 849 (2013).
- [69] G. Ódor, *Universality in Nonequilibrium Lattice Systems: Theoretical Foundations* (World Scientific, 2008), ISBN 9789812812278.
- [70] G. Ódor, B. Liedke, and K.-H. Heinig, Phys. Rev. E **81**, 031112 (2010).